Thermal Decomposition of Co-Doped Calcium Tartrate and Use of the Products for Catalytic Chemical Vapor Deposition Synthesis of Carbon Nanotubes.

Igor P. Asanov, Tatyana I. Asanova, Lyubov Gennadievna Bulusheva, Elena V. Shlyakhova, Alexander Vladimirovich Okotrub, Emmanuel Flahaut

DOI:10.1021/jp2092169
Official URL: http://dx.doi.org/10.1021/jp2092169

Thermal Decomposition of Co-Doped Calcium Tartrate and Use of the Products for Catalytic Chemical Vapor Deposition Synthesis of Carbon Nanotubes

Igor P. Asanov,[†] Tatyana I. Asanova,[†] Lyubov G. Bulusheva,[*,†] Elena V. Shlyakhova,[†] Alexander V. Okotrub,[†] and Emmanuel Flahaut[‡,§]

[†]Nikolaev Institute of Inorganic Chemistry, SB RAS, 3 Academician Lavrentiev Avenue, Novosibirsk, 630090, Russia

[‡]Institut Carnot Cirimat, Université de Toulouse, UPS, INP, 118, route de Narbonne, F-31062 Toulouse cedex 9, France

[§]Institut Carnot Cirimat, CNRS, F-31062 Toulouse, France

ABSTRACT: Thermal decomposition of Co-doped calcium tartrate in an inert atmosphere or air was studied using thermogravimetric analysis and X-ray absorption fine structure (XAFS) spectroscopy. It was shown that the powder substance containing 4 at.% of cobalt completely decomposes within 650−730 °C, depending on the environment, and the formation of Co clusters does not proceed before 470 °C. The products of decomposition were characterized by transmission electron microscopy, XAFS, and X-ray photoelectron spectroscopy. Surface-oxidized Co metal nanoparticles as large as ∼5.6 ± 1.2 nm were found to form in an inert atmosphere, while the annealing in air led to a wide distribution of diameters of the nanoparticles, with the largest nanoparticles (30−50 nm) mainly present as a Co_3O_4 phase. It was found that the former nanoparticles catalyze the growth of CNTs from alcohol while a reducing atmosphere is required for activation of the latter nanoparticles. We propose the scheme of formation of CaO-supported catalyst from Co-doped tartrate, depending on the thermal decomposition conditions.

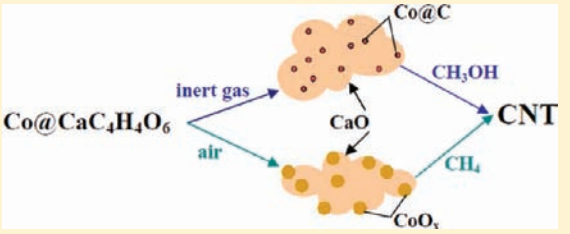

INTRODUCTION

Carbon nanotubes (CNTs) present a class of one-dimensional carbon cages characterized by a variety of number of the constituting graphitic layers, outer diameter, defectness, morphology, etc. Depending on the structural and physicochemical properties, each kind of CNT could find its own application.[1] For example, single-wall CNTs are considered as elements of nanoelectronics and optical devices, highly defective CNTs can be used as effective sorbents and supports, and few-wall CNTs are attractive as reinforcement additives in composites. The structure of CNTs can be tuned, varying the synthesis parameters. A major processing route toward the CNTs in mass production is catalytic chemical vapor deposition (CCVD), where carbon-containing molecules decompose at a catalyst surface.[2] Catalyst, which commonly consists of a compound of one or two transition metals,[3] is a key parameter in the CCVD due to a rigorous correlation between the diameter of CNTs and size of metallic particles.[4,5] Despite numerous works devoted to the study of CNT morphology as a function of catalyst composition and structure,[6−10] the dependences are still not very clear. Researchers believe that understanding mechanisms of CNT growth, particularly the role of chemical oxidation state of catalyst in the CCVD process, should allow the production of CNTs with the required characteristics, depending on the desired application.[11]

One of the important problems hindering the control of the size and crystallinity of catalyst is an agglomeration of metallic nanoparticles at elevated temperatures of synthesis.[12] To restrict the nanoparticle enlargement, the metal is deposited on a substrate, though the catalyst−substrate interaction also exerts an influence on particle coalescence and thus on the nanotube growth.[13−16] For substrate material, inorganic compounds with high specific surface area such as Al_2O_3, SiO_2, MgO, CaO, and $CaCO_3$ are used.[17−21] The latter three compounds have an advantage over the other substrates because alkaline-earth metal oxide can be easily removed from the synthesis product by dissolution with a weak acid treatment.[22,23] An often-used method for the formation of catalytic nanoparticles is the impregnation of powder substrate by transition metal salt solution.[24] Activation of the catalyst arises from the heating process followed by reduction. For $CaCO_3$ substrate, all these pretreatment steps occur directly in the reactor,[25] which simplifies the CCVD process.

We have suggested that doped salts containing both alkaline-earth metal and transition metal could be suitable precursors for supported catalysts for the CNT formation and checked the idea on the example of calcium tartrate.[26] The pure and doped

dx.doi.org/10.1021/jp2092169

calcium tartrate crystals owing to their electrical properties are employed in transducers and many linear and nonlinear mechanical devices.[27,28] They can be also used as catalysts for asymmetric synthesis and as chiral intermediates.[29] The structure of doped calcium tartrate crystals was studied by Torres et al.,[30] who showed that ions of a transition metal occupy interstitial sites in the host lattice. Thermal stability of pure calcium tartrate or with impurities depends on the crystal perfectness, and the conversion to calcium oxide is completed between 420 °C and 807 °C,[31,32] which is close to the CCVD operation temperature. On the basis of these data, we hoped that the decomposition of calcium tartrate doped with transition metal may result in monodisperse catalyst nanoparticles supported over CaO. Our investigations indicated that the limiting concentration of transition metal in calcium tartrate lattice is ~4 at.%, and after thermal decomposition in the inert atmosphere, the average size of supported catalyst nanoparticles is ~6 nm.[33] Feeding the ethanol to the CCVD reactor just after precursor decomposition in an inert atmosphere gave thin multiwall CNTs with narrow outer diameter distribution determined by the size of the Co nanoparticles. However, the mechanism of the formation of metallic nanoparticles catalyzing the CNT growth remained unclear.

Here, using the example of Co-doped calcium tartrate, we undertake a study of changing the oxidation state of transition metal with thermal decomposition of the salt using in situ X-ray absorption fine structure (XAFS) measurements additionally to the methods of high-resolution transmission electron microscopy (HRTEM), thermogravimetry (TG), and X-ray photoelectron spectroscopy (XPS). The products obtained in air or inert atmosphere are examined as catalytic systems for growth of CNTs from a specific feedstock. Suggestions about how the conditions of doped calcium tartrate decomposition influence the structure of CNTs are made.

EXPERIMENTAL SECTION

Synthesis and Decomposition of Calcium Tartrate Doped with 4 at.% Co. Co-doped calcium tartrate was synthesized by the procedure described elsewhere.[33] Co acetate and Ca chloride were used as metal sources. The sodium tartrate solution was added to the solution containing cobalt and calcium ions (the theoretical ratio of Co to Ca was 1:9). The precipitation of doped calcium tartrate was a result of the following reaction: $Na_2C_4H_4O_6 + CaCl_2 + Co(CH_3COO)_2 \cdot 4H_2O \rightarrow Ca_{1-x}Co_xC_4H_4O_6 \cdot 4H_2O\downarrow + NaCl + NaCH_3COO$. The precipitate was filtered and repeatedly washed with deionized water and then dried in air at ambient conditions. The obtained pink fine powder was decomposed in an argon atmosphere or in air. It was expected that the first method should lead to nanosized Co particles distributed in the CaO matrix in agreement with the reaction $Ca_{1-x}Co_xC_4H_4O_6 \rightarrow CaO + Co + CO_2 + H_2O$. The product obtained by this method is labeled syst1. The formation of syst1 was performed within the CCVD reactor just before the CNT synthesis. The other catalytic system was prepared by decomposition of doped tartrate in air at 800 °C for 30 min. In this case, the formation of a mixture of Co and Ca oxides was expected as a result of the following reaction: $Ca_{1-x}Co_xC_4H_4O_6 + O_2 \rightarrow CaO + Co_xO_y + CO_2 + H_2O$. The product of this synthesis is labeled syst2.

CNT Synthesis. CNT synthesis was carried out in a horizontal quartz tube. The reactor chamber was pumped out and heated up to 800 °C. Then Ar flow (200 mL/min) was supplied, and a boat loaded with the Co-doped calcium tartrate was moved to the hot zone of the reactor and heated for 10 min to obtain syst1. The duration of the precursor decomposition in the reactor as well as temperature of synthesis of few-walled CNTs was optimized in ref 33. CNT growth was performed under ethanol vapor pressure of ~65 mbar for 60 min. At the end of the synthesis, the carbon source feed was stopped and the reactor was cooled to room temperature in an inert gas flow. The product obtained was a black, friable substance labeled as cnt1. The synthesis of CNTs using methane as a carbon source was performed according to the method previously reported for double-walled CNT synthesis.[34] The boat loaded with syst2 was inserted in the reactor chamber which was then heated up to 1000 °C at the rate of 5 °C/min in the H_2-CH_4 (18 mol % CH_4) flow. The reactor was cooled to room temperature at the same rate. The synthesis product obtained from methane using the catalytic system syst2 is denoted as cnt2.

Characterization Techniques. Thermogravimetric (TG) decomposition patterns of Co-doped calcium tartrate were measured in He flow (150 mL/min) or in air on a Q-1000 derivatograph. The heating rate was 10 °C/min. The yield of CNTs was estimated by means of scanning electron microscopy (SEM) on a JEOL JSM-6700 F microscope. TEM characterization was performed on a JEM-2010EX transmission electron microscope. Fourier analysis of TEM images was used to estimate the interplanar distances and identify crystal structures. Energy dispersed X-ray (EDX) analysis was performed on a spectrometer (Phoenix) with a Si(Li) detector at an energy resolution of ~130 eV and a probe size of 10 nm. Room-temperature Raman spectra were measured using the Ar laser lines at 488 and 514.5 nm and HeNe laser line at 633 nm on a Triplemate spectrometer.

The in situ high temperature Co K-edge XAFS spectra of the Co-doped calcium tartrate as well as ex situ spectra of the samples were measured at the 7C1 beamline PLS POSTECH (Pohang Light Source, Republic of Korea) with a ring electron current of 120−170 mA at 2.0 GeV. A Si (111) double-crystal monochromator with an energy resolution of $\Delta E/E = 2 \times 10^{-4}$ was used. The ex situ XAFS spectra were recorded in a fluorescence mode while in situ XAFS spectra were in transmission mode. In the in situ XAFS experiment, the sample was heated to the required temperature for 10 min and then stabilized for the next 10 min. Temperatures of 200 °C, 370 °C, 470 °C in air or 200°, 400 °C in He atmosphere were chosen as corresponding to the thermal decomposition stages. IFEFFIT computer program[35,36] was employed for analysis of XAFS data.

XPS measurements were carried out on a Specslab PHOIBOS 150 spectrometer using Al $K\alpha_{1,2}$ (1486.6 eV) X-ray radiation in vacuum (1.3×10^{-7} Pa) at room temperature. The binding energies were measured relative to the C 1s level (285.0 eV) from surface hydrocarbon contaminations.

RESULTS

Study of Co-Doped Calcium Tartrate and Products of Its Thermal Decomposition. *Thermogravimetric Analysis.* TG curves for the Co-doped calcium tartrate in He atmosphere and air are compared in Figure 1. In both cases it is possible to denote four stages of the thermal decomposition of the salt that agree with data for undoped calcium tartrate.[32] Because the concentration of Co atoms in the host lattice is about 4 at.% according to the chemical analysis, the main weight loss of the samples can be assigned to the calcium tartrate decomposition described by the reactions mentioned below. In the first two stages we observe

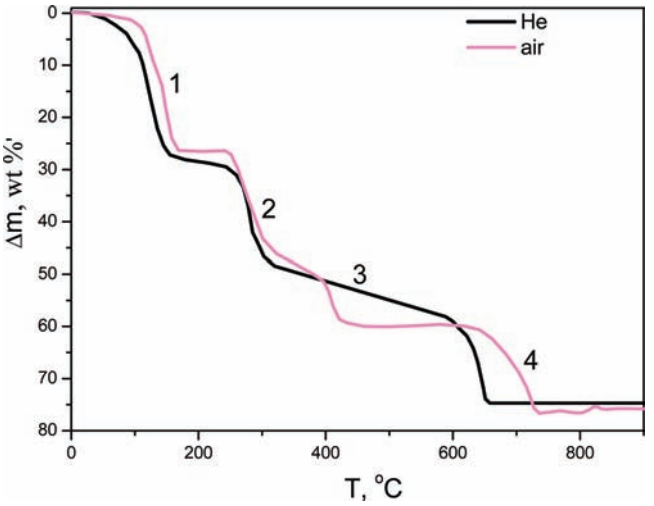

Figure 1. Thermal gravimetric (TG) curves of decomposition of Co-doped calcium tartrate in air and He atmosphere. The numbers indicate the stage of decomposition.

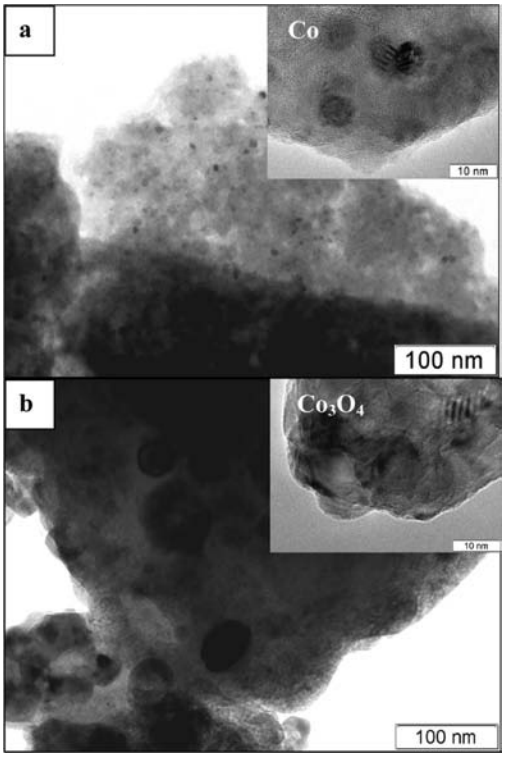

Figure 2. TEM images of products of decomposition of Co-doped calcium tartrate in inert (a) and air (b) atmosphere. The inserts show high-resolution images of nanoparticles.

almost no difference between the decomposition processes in the different environments. The weight loss occurring in the region 60−206 °C is attributed to the crystallization water removal (27 wt % theoretically) according to the reaction $CaC_4H_4O_6 \cdot xH_2O \xrightarrow{-xH_2O} CaC_4H_4O_6$. The water stoichiometry in doped calcium tartrate estimated from the TG data is 4. The second stage at 246−322 °C is assigned to the transformation of the tartrate into oxalate (23 wt % theoretically) by the reaction

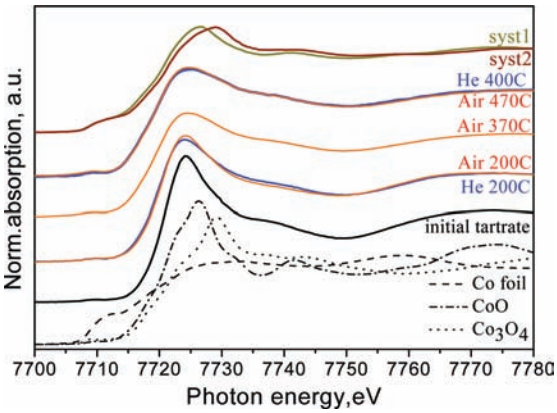

Figure 3. Co K-edge XANES of Co-doped calcium tartrate, heated in air at 200 °C, 370 °C, and 470 °C or in He at 200 °C and 400 °C and products of final decomposition of the tartrate in inert atmosphere (syst1) or in air (syst2) in comparison with the spectra of reference samples Co foil, CoO, and Co_3O_4.

$CaC_4H_4O_6 \xrightarrow{-2H_2O,\ -2C} CaC_2O_4$. The main distinctions between the measured curves are obtained in the third stage, in the range 372−487 °C. Here it is assumed that the transformation of oxalate into carbonate proceeds according to $CaC_2O_4 \xrightarrow{-CO} CaCO_3$. The weight loss in He atmosphere and air is 6 wt % and 11 wt %, respectively. We assign the larger weight loss and the exothermal effect observed in differential thermal analysis (DTA) (part b of Figure S1 in Supporting Information) with tartrate decomposition in air to the reaction $C + O_2 \rightarrow CO_2$. The delayed weight loss in the case of the third stage of the decomposition in He atmosphere can be attributed to a slow burning of the carbon-containing phase in the presence of oxygen traces in the inert gas (purity 99.995). The last stage is associated with the conversion of carbonate to the oxide according to $CaCO_3 \xrightarrow{-CO_2} CaO$ (17 wt % theoretically). The difference in the final temperatures of the tartrate decomposition in He atmosphere and air (~650 and 730 °C) is probably related to the larger agglomeration of $CaCO_3$ particles in air conditions.

TEM Study of Thermal Decomposition Products. A typical TEM image of the product of Co-doped calcium tartrate decomposition in an inert atmosphere (syst1) is presented in Figure 2a. According to EDX data (Figure S2 in Supporting Information), the dark brown powder is a nanocomposite of CaO and Co nanoparticles (the dark inclusions in the image). Statistical analysis of TEM images revealed that the size of Co nanoparticles is uniform and ranges between 1.3 and 8.9 nm, with an average value of 5.6 nm. TEM study of the syst2 sample showed that the size distribution of the nanoparticles formed in the CaO matrix varies over quite a wide range from 30 to 180 nm (Figure 2b). To identify the structure of the nanoparticles, the interplanar distances were determined by Fourier transform (FT) analysis of HRTEM images. It was found that the nanoparticles in the syst1 sample are mainly composed of metallic Co and a small portion of CoO. In the syst2 sample the nanoparticles with a composition of Co_3O_4 are the most abundant, while a few CoO and Co nanoparticles are also detected. The presence of Co nanoparticles in the nanocomposites is due to the CaO matrix, which can protect metallic nanoparticles from oxidation in air.

XAFS Study. Co K-edge XANES spectra of the Co-doped calcium tartrate and products of its thermal decomposition in He or air are shown in Figure 3 together with the spectra of reference

Table 1. EXAFS Parameters for Co-Doped Calcium Tartrate, Product of Its Thermal Decomposition in Air (syst2) and Products of CCVD Synthesis of CNTs Using syst1 and syst2 Samples As the Catalytic Systems: *R*, Interatomic Distance; σ^2, Debye−Waller Factor; *N*, Coordination Number; *R*-Factor, Quality of the Fit

	coordination shell	*R*, Å	σ^2, Å^2	*N*	notes	*R*-factor, %
tartrate	Co−O	2.088 (9)	0.0055 (6)	6.2 (2)		1
syst2	Co−O	1.882 (4)	0.004 (3)	3 (1)	O from Co_3O_4	2
	Co−Co	3.333 (7)	0.012 (6)	8 (4)	Co from Co_3O_4	2
	Co−Co	2.518 (9)	0.005 (1)	4 (1)	Co metal	2
cnt1	Co−Co	2.494 (4)	0.0074 (6)	11.0 (5)	Co metal	1
	Co−Co	3.526 (6)	0.0108 (9)	5.5 (2)	Co metal	1
	Co−Co	4.319(8)	0.011 (1)	22.1 (9)	Co metal	1
	Co−Co	4.987 (9)	0.011 (1)	11.0 (5)	Co metal	1
cnt2	Co−Co	2.504 (4)	0.0069 (4)	11.8 (5)	Co metal	1
	Co−Co	3.541(6)	0.0088 (4)	4.7 (2)	Co metal	1
	Co−Co	4.336 (7)	0.009 (1)	23.5 (9)	Co metal	1
	Co−Co	5.008 (8)	0.009 (1)	11.8 (5)	Co metal	1

compounds Co foil, CoO, and Co_3O_4. The spectrum of the initial tartrate shows the high intensity of the main peak after the absorption edge, the so-called "white line", that is typical for CoO, Co_3O_4, and $LiCoO_2$. The energy position of the edge is similar to that of CoO. FT EXAFS spectrum shows a single peak at ∼1.6 Å (Figure S3 in Supporting Information), which most probably corresponds to an oxygen coordination shell. Indeed, according to the data obtained from the fitting procedure this shell consists of six oxygen atoms and has a radius of ∼2.09 Å (Table 1). This radius is also characteristic for CoO (2.13 Å). The obtained radius and coordination number of Co−O shell indicates that cobalt atoms are located in vacant interstitial sites in calcium tartrate lattice. Otherwise, if Co atoms had been substituted with Ca atoms, the average radius and coordination number would have been ∼2.4 Å and 8, respectively, similar to that of the Ca−O shell in calcium tartrate.[37]

Co K-edge XANES spectra of the Co-doped calcium tartrate heated in situ up to temperatures corresponding to stages 1−3 in the process of thermal decomposition show the insignificant differences between the samples measured in air and the inert atmosphere (Figure 3). When the temperature is increased, the intensity of the "white line" decreases. This probably arises from the decrease in the first coordination number of Co. The estimations of EXAFS parameters for the products in the third stage (400 °C in inert atmosphere and 470 °C in air) are also in favor of this assumption. Co−O coordination numbers were estimated to be 3.2 (3) and 3.8 (4) for the product obtained in air and the inert atmosphere, respectively, while the radius of the shell is approximately the same for both products ∼1.98 (1) Å. In all the spectra the pre-edge peak at 7710 eV and the energy positions of the Co K-edge are constant over the measured temperature range. Thus, the oxidation state of Co in the sample equals +2, and it is not changed in the products of thermal decomposition in different environments up to 470 °C. Note that the spectra measured in air at 370 °C and 470 °C and in He atmosphere at 400 °C have gently sloping absorption edges, and they are considerably different from those measured at the temperature (200 °C) characteristics of the first stage of decomposition of Co-doped calcium tartrate. A gently sloping edge is typical for samples having an absorbing atom in several oxidation states or interacting with different types of atoms (for example Co−O and Co−C).

Co K-edge XAFS spectra show that complete thermal decomposition of doped tartrate in the inert atmosphere and air yields the different resultant products syst1 and syst2 (Figure 3). In addition to the low-intensity "white line", these spectra have a feature typical for metallic cobalt, indicating that the resultant products consist of metallic cobalt and cobalt oxides. The spectrum of syst2 shows a shift to the higher energy compared to that of syst1. The difference in the shape of the "white line" can also be observed in the spectra of syst1 and syst2. These distinctions can originate from nanoparticles with several composite structures or several phases, and their different ratio in the sample. Three peaks detected in the FT EXAFS spectrum of syst1 and syst2 samples in a range from 1.0 to 3.3 Å (Figure S3) are due to Co−O (∼1.4 Å) and two Co−Co interactions, one of which originated from Co metal (2.1 Å) and the other one from cobalt oxide (∼2.7−2.9 Å). The FT peaks of syst2 were well described using a combination of two structures, metallic Co and Co_3O_4, with a ratio of 2.3:1. The obtained EXAFS parameters are collected in Table 1. However, the best model to fit the experimental FT of syst1 was not found. It mostly deals with the presence of several structures/phases (more than two) in the sample. In this case many EXAFS parameters should be included in the fitting. This approach can improve the agreement between the theoretical and experimental spectra but makes EXAFS parameters unreasonable. The low value of the Co−O coordination number for syst2 could result from a thin surface layer of cobalt oxide on the metallic Co nanoparticles. FT peaks in the range of 3.3−5.4 Å may be attributed to long-distance Co−Co coordination shells.

XPS Study. The XPS survey spectrum of the Co-doped calcium tartrate (part a of Figure S4 in Supporting Information) detected the signals of carbon, oxygen, calcium, and cobalt. The concentration of Ca at the sample surface (without considering hydrogen atoms) calculated from the XPS spectrum is 7 at.%; the atomic ratio Co/Ca is 0.04. Two peaks at 286.7 and 288.7 eV in the C 1s spectrum of the sample correspond to carbon atoms bonded with hydroxyl groups and carbon atoms in carboxyl groups. Oxygen atoms of these groups contribute to the O 1s spectrum components located at 533.2 and 531.8 eV with an intensity ratio of 1:2 (part b of Figure S4 in Supporting Information). The Co $2p_{3/2}$ line is centered at 780.6 eV and has a broad, intensive satellite line at a distance of 4 eV from the higher binding energy (Figure 4). The spin−orbital splitting

Co $2p_{3/2-1/2}$ is 14.7 eV. Such a Co 2p spectrum indicates that cobalt atoms are in the Co (+2) charge state in an octahedral oxygen environment. These results agree well with XAFS data.

For the syst1 and syst2 samples, XPS revealed the presence of calcium carbonates and a 2-fold increase in concentration of calcium on the surface compared to that of initial tartrate (Figure S5 in Supporting Information). In addition, the surface concentration of carbon atoms at 285 eV is higher in the syst1 sample than in the syst2 one, which could be due to incomplete burning of carbon in syst1 in agreement with the TG result. The surface Co concentration in syst1 is unchanged compared to that of the initial tartrate while it is three times higher in the syst2 sample. The binding energies of $Co2p_{3/2}$ levels are 781.0 and 780.4 eV for syst1 and syst2, respectively, and intensity of the satellite considerably decreases and shifts to higher energy as compared to that in the XPS spectrum of the initial tartrate (Figure 4). These data indicate the formation of Co_3O_4 on the surface of the samples.[38] It is worth noting that in the syst1 spectrum the $Co2p_{3/2}$ peak is shifted to higher binding energy and the satellite intensity is higher than that in the syst2 spectrum, which could be related to covering of the cobalt nanoparticles by oxides that are intermediate between CoO and Co_3O_4. This is consistent with TEM and XAFS conclusions about the incomplete oxidation of Co in syst1. Note that metallic cobalt was not detected in syst1 and syst2 while the photoelectrons with the used kinetic energy probed the samples with a penetration depth of ~3 nm.

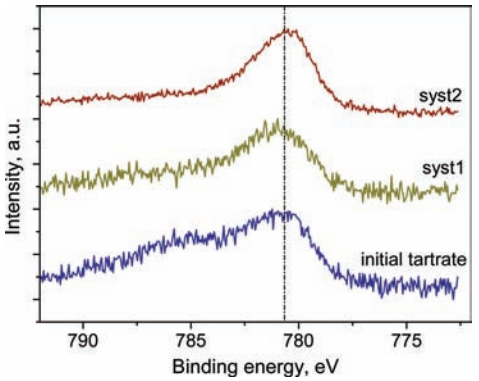

Figure 4. XPS spectra of the Co $2p_{3/2}$ level for Co-doped calcium tartrate and products of its decomposition in Ar atmosphere (syst1) or in air (syst2).

Study of Products of CCVD Synthesis. *Structural Characterization.* SEM and TEM images of the products of CCVD synthesis resulting from the decomposition of ethanol vapors or methane using catalytic systems syst1 or syst2 are presented in Figure 5. According to TEM and XPS data after inserting the Co-doped calcium tartrate in the reaction zone of CVD reactor and its decomposition in Ar atmosphere at 800 °C for 10 min, surface-oxidized Co nanoparticles were formed in the CaO matrix (syst1 sample). Decomposition of ethanol vapors on these nanoparticles produced CNTs (Figure 5a,b). TEM study of the cnt1 sample showed formation of multiwall CNTs with an outer diameter ranging from 4 to 21 nm and a mean value of ~10 nm (Figure 5b). The measurement of the metallic particles present in the carbon material detected that their average diameter increased to 6.7 nm, which is indicative of the aggregation process at 800 °C during the CNT growth. In the case of ethanol decomposition over the syst2 sample, where the catalytically active atoms are mainly as Co_3O_4, formation of a very limited number of CNTs among the agglomerates of CaO was observed (part a of Figure S6 in Supporting Information).

Thermal decomposition of the Co-doped calcium tartrate immediately under the conditions of the reduction atmosphere

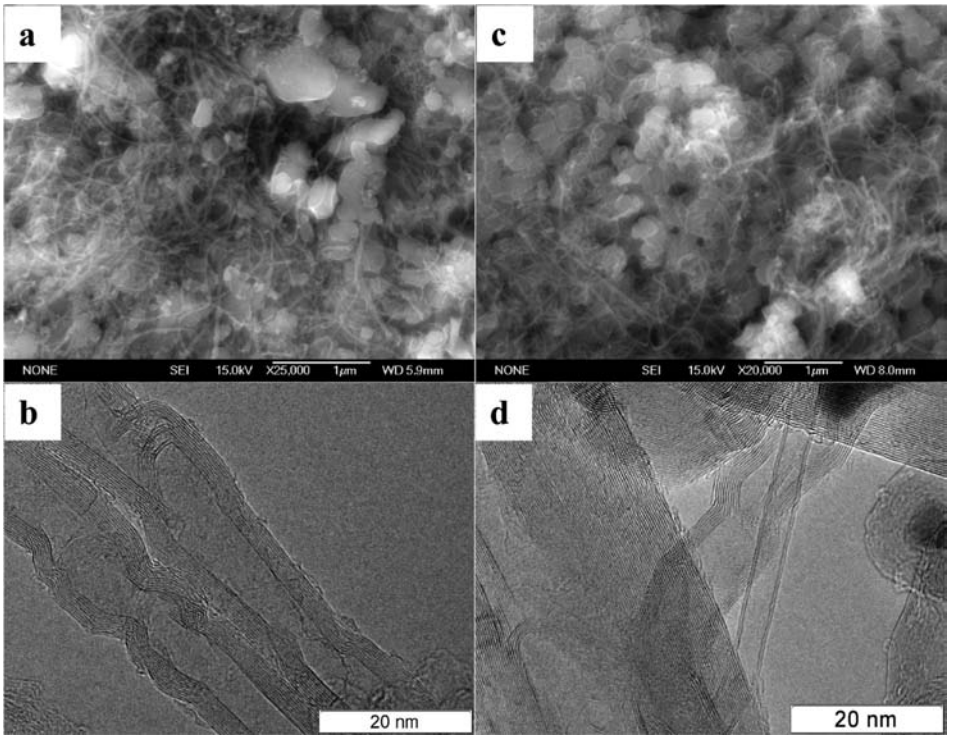

Figure 5. SEM (a) and HRTEM (b) image of sample produced by C_2H_5OH decomposition over syst1 at 800 °C. SEM (c) and HRTEM (d) image of sample produced by CH_4 decomposition over syst2 at 1000 °C.

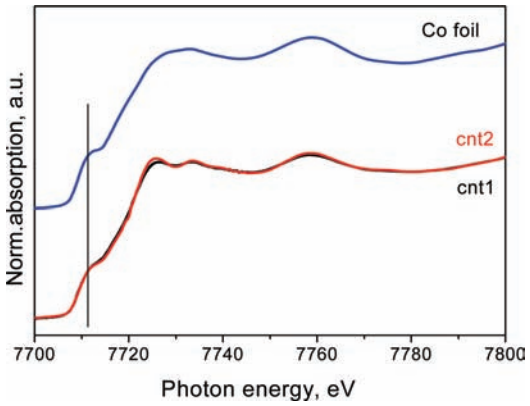

Figure 6. Co K-edge XANES of CCVD products of C_2H_5OH decomposition over syst1 (cnt1) and CH_4 decomposition over syst2 (cnt2) in comparison with the spectrum of Co foil.

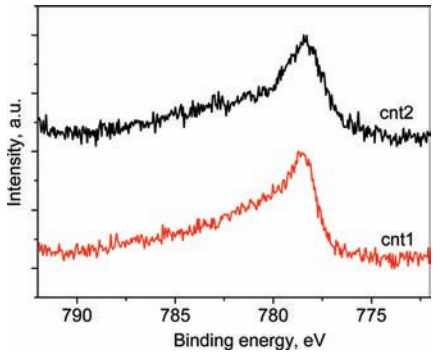

Figure 7. XPS spectra of Co $2p_{3/2}$ level for CNT samples synthesized by C_2H_5OH decomposition over syst1 (cnt1) and CH_4 decomposition over syst2 (cnt2).

(CH_4-H_2) produced an extremely limited number of CNTs (part b of Figure S6). The size of metallic particles formed during the in situ decomposition of tartrate in the reactor is more likely to be insufficient to nucleate CNTs, and decomposition of methane mainly yields amorphous carbon. Alternatively, using syst2 under the same conditions resulted in the formation of CNTs (Figure 5c) in an amount comparable with the decomposition of ethanol over syst1 (Figure 5a). TEM analysis revealed a large variation of CNTs in diameter, and the occurrence of a double-walled CNT with ~4 nm outer diameter, in addition to the thick ~60 nm CNTs (Figure 5d). Most CNTs in sample cnt2 are ~20 nm in diameter.

The structural peculiarities of the samples cnt1 and cnt2 derived from the TEM analysis were supported by Raman spectroscopy. An increase in the number of walls in the CNTs composing the cnt2 sample resulted in better graphitization of the layers and narrowing of the D mode resonance[39] as compared to the spectrum of cnt1 sample (Figure S7 in Supporting Information). The average outer diameter of CNTs was estimated from the frequency of the G mode, which has been shown to decrease with the multiwall CNT diameter increasing.[40] The values 1594 cm^{-1} for cnt1 and 1587 cm^{-1} for cnt2 correspond to CNTs with the diameters less than 10 nm in the former sample and in the range 10−20 nm in the latter one. The peaks detected in the radial breathing mode (RBM) region of the Raman spectrum of the cnt2 sample could correspond to single-walled CNTs or the inner tubes of double-walled CNTs. Diameters of these nanotubes were calculated using the equation from ref 41 to be within 1.2−1.8 nm. A ratio of different carbon species in the cnt2 sample was evaluated from the TG data (Figure S9 in Supporting Information). The major part of the sample (~85%) is multiwall CNTs burning around 630 °C,[8] the quantity of double-walled and single-walled CNTs destroyed within 430−520 °C[42,43] is about 8%, and the rest of the carbon likely corresponds to amorphous species.

XAFS and XPS Investigation of CCVD Products. Co K-edge XANES spectra of samples cnt1 and cnt2 and Co foil as a reference compound are compared in Figure 6. The spectra of the produced samples are similar in appearance and notably different from that of metallic Co, particularly, the first peak after the absorption edge is much better resolved in energy in the spectra of samples cnt1 and cnt2. Similar Co K-edge XAFS spectra have been observed for bimetallic nanoparticles AgCo[44] and PdCo,[45] where Co replaced the Ag/Pd position in a face-centered cubic (fcc) structure. It is well-known that the structure of metallic Co has three different forms: hexagonal hcp (α-phase), cubic fcc (β-phase), and primitive cubic (ε-phase).[46−48] The β-phase commonly occurs in nanoparticles with a size less than 20 nm[49] and in bulk at temperatures higher than 422 °C. FT EXAFS of the samples cnt1 and cnt2 (Figure S10 in Supporting Information) show all peaks typical for Co foil although the difference in the amplitude of the peaks is clearly seen. To determine the local atomic parameters of Co in the samples, the fitting in the range 1.2−5.1 Å was carried out with the β- and α-phase structures as initial models. The best model was found to be the β-structure. The obtained local atomic parameters of Co in the samples cnt1 and cnt2 are listed in Table 1. The smaller effective coordination number is obtained for cnt1 (~11), for which FT peaks also show the smallest amplitude. All of these are results of a size effect. Thus, the average particle size is smaller for cnt1, which agrees well with TEM results.

XPS Co $2p_{3/2}$ spectra of cnt1 and cnt2 are compared in Figure 7. A major peak at ~778.5 eV corresponds to atoms of metallic Co nanoparticles.[50,51] A shoulder at 780.5 eV is associated with Co oxides. The integral intensity of this shoulder is higher in the spectrum of cnt2, which indicates a higher surface concentration of Co oxide. Thus, regardless of the initial state of metal atoms in the catalytic systems syst1 and syst2, the products of CCVD synthesis (cnt1 and cnt2) mainly consist of metallic Co nanoparticles and some amount of Co oxides. The presence of the latter species in CCVD products probably is related to the surface oxidation of non-carbon-encapsulated metallic nanoparticles under the conditions of laboratory storage.

DISCUSSION

Experimental data presented above allowed us to propose a scheme of transformations of the Co-doped calcium tartrate under heating in inert or oxidizing atmosphere and of the obtained mixed metal oxide systems during the process of CCVD synthesis of CNTs using a specific feedstock (Figure 8).

XAFS data showed that the doping of calcium tartrate with Co atoms results in the formation of an interstitial solid solution. Therefore, Co atoms are separated from each other and uniformly distributed in the interstices of the calcium tartrate lattice. On the basis of this structural model, it might be expected that under heating, Co atoms are able to move easily and form metallic nanoparticles. However, according to the

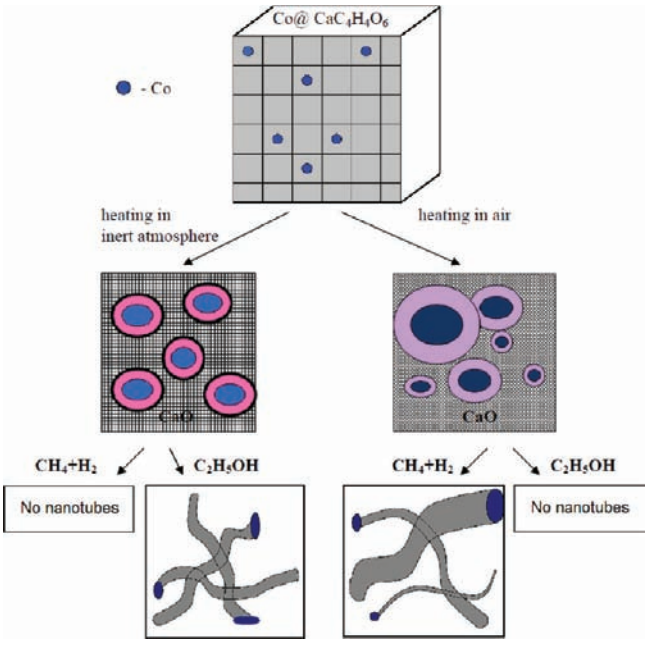

Figure 8. Scheme of transformation of Co-doped calcium tartrate under heating in inert atmosphere or in air and of the CaO-supported metallic nanoparticles in the CCVD process utilizing specific feedstock (ethanol or $CH_4 + H_2$).

temperature-dependent EXAFS study, Co atoms are coordinated with oxygen atoms up to 470 °C, and agglomeration of the atoms happens only at the last stage of thermal decomposition of the tartrate (above 610 °C). The formed nanoparticles mainly consist of Co and Co_3O_4, while in the sample obtained by the thermal decomposition in the inert atmosphere (syst1), there are additional components unidentified by this method. They may be related to interface states forming between the Co metallic core and the oxide shell.

TEM images of the decomposition products showed that the Co nanoparticles and its oxides are dispersed in a CaO matrix. The diffraction pattern of the nanoparticles obtained by HRTEM corresponds to Co and CoO phases in syst1 and Co, CoO, and Co_3O_4 phases in syst2 (the decomposition in air). Note that TEM is a local method, providing information only for a small portion of the sample. XPS study of both samples only revealed the oxidized state of Co (Co_3O_4 in syst2 and oxides being intermediate between CoO and Co_3O_4 in syst1), indicating the encapsulation of the Co core into the oxide shell. During preparation of syst1, oxygen required for formation of oxides can come from calcium tartrate as well as an impurity in the inert gas. The size distribution of the Co nanoparticles in the decomposition products strongly depends on the heating atmosphere. In syst1 the nanoparticle size varies from 1.3 to 19 nm, while in syst2 the nanoparticles are much larger and reach 30−180 nm. Perhaps the wide range of the particle sizes obtained by the thermal oxidation of the Co-doped calcium tartrate is also related to the different cobalt compositions in syst2.

According to XPS, the surface of syst1 is enriched in carbon as compared to that of syst2. From TG data, the carbon excess in the product of the decomposition of Co-doped calcium tartrate in the inert atmosphere may be due to a deficiency in oxygen in the tartrate lattice to completely burn carbon. We suggest that the excess carbon forms a shell around nanoparticle, which prevents an uncontrolled cobalt agglomeration, observed in syst2. The effective growth of CNTs from ethanol using syst1 in the CCVD process can be attributed to the formation of a metallic nanoparticle surface during the burning of the carbon shell. In the absence of oxygen in the feedstock, only a small amount of CNTs is observed in the synthesis product. To remove oxygen from nanoparticles in syst2, a reducing atmosphere is required. This is evidenced by the formation of CNTs from CH_4-H_2 and their almost complete absence in the sample where alcohol, containing a small amount of active hydrogen, was used as the carbon source.

After CCVD syntheses of CNTs in both samples obtained by using the catalytic systems syst1 or syst2, the metallic Co nanoparticles have an fcc structure (β-phase). According to XPS data, the nanoparticles' surface is coated with CoO, the relative amount of CoO being much higher in the case of the use of syst2 for CNT growth. The presence of CoO in CCVD products could be due to an interaction of Co with oxygen from calcium tartrate.[52] It is possible if the catalytic nanoparticles have a strong bond with the CaO matrix. The possibility must not be ruled out that CoO covers Co nanoparticles located inside the nanotubes. In this case it would be necessary to further investigate the role of cobalt oxide in the process of CNT growth.

TEM images of the products of thermal decomposition of Co-doped calcium tartrate and CNTs formed with the use of these products showed a correlation between the metallic nanoparticles size and the nanotubes diameter. However, in case of CCVD synthesis using syst2 containing numerous large metallic nanoparticles (30−180 nm), small-diameter CNTs, particularly, double-walled nanotubes and probably single-walled nanotubes, were obtained. The reason for this could lie in the reduction process of cobalt oxides. The reduction of a large nanoparticle can run nonuniformly. Because in our case the carbon source is supplied to the surface of the oxidized nanoparticle simultaneously with hydrogen, the growth of small-diameter CNTs on the reduced area of the metal nanoparticles can be expected. It is also possible that the small-diameter CNTs could result from catalysis by small-diameter Co nanoparticles formed in situ in addition to the large-diameter nanoparticles already present.

CONCLUSIONS

A study of the thermal decomposition of Co-doped calcium tartrate in an inert atmosphere and air has been performed using TG analysis and in situ XAFS experiments. The XAFS investigations showed that Co atoms are isolated from each other and occupy interstitial sites in the calcium tartrate lattice. Formation of metallic Co nanoparticles occurs during the last stage of thermal decomposition of the tartrate above 500 °C independently on the environment. The nanoparticles have narrow distribution in diameter when decomposition proceeds in an inert atmosphere and the reason for this according to TG and XPS data is the incomplete burning of carbon contained in the tartrate. Abundant carbon forms a shell around Co nanoparticles and thereby prevents uncontrolled agglomeration of the nanoparticles. To remove this shell for activation of the metallic catalyst, the presence of oxygen-containing compounds is necessary in the CVD process. Therefore, from ethanol, CNTs are formed while from methane, CNTs do not practically grow. On the contrary, with the use of the thermal decomposition product obtained in air, CNT growth occurs only in a reducing atmosphere. After CCVD synthesis, an fcc structure of Co in the nanoparticles is formed which does not depend on the cobalt state in the catalytic system.

The results from this study reveal that varying the conditions of thermal decomposition of calcium tartrate doped with transition metal allow the change in size and chemical state of forming metallic nanoparticles. These nanoparticles distributed in CaO can be used as catalysts for the CCVD growth of different kinds of CNTs. We showed that catalysts can produce very defective few-walled CNTs, multiwall CNTs with high crystallinity of graphitic layers, and even double-walled and probably single-walled CNTs. A specific characteristic of the CCVD products is the nonbundling of CNTs, and such dispersive material could find application as fillers in various composites. Furthermore, we believe that alkali-metal tartrates (Ca, Mg, Ba, and their mixtures) doped with transition metals (Ni, Co, Fe, and their mixtures) will decompose, following a mechanism determined for the Co-doped calcium tartrate that would open possibilities for creation of new materials, particularly, carbon-encapsulated transition metal nanoparticles or supported catalysts for CNT growth.

■ ASSOCIATED CONTENT

Supporting Information. Figure of TG, DTG, and DTA curves, HRTEM image and EDX analysis of the product of thermal decomposition of Co-doped calcium tartrate, Fourier transform of the experimental $k^2\chi(k)$ Co K-edge EXAFS and fits for the initial Co-doped calcium tartrate and products of its decomposition, figure of XPS spectra, figure of SEM images, Raman spectra, TG, DTG, and DTA analysis, and Fourier transform of the experimental $k^2\chi(k)$ Co K-edge EXAFS and fit for the CCVD products of CH_4 or C_2H_5OH decomposition over the catalytic systems syst1 and syst2. This material is available free of charge via the Internet at http://pubs.acs.org.

■ AUTHOR INFORMATION

Corresponding Author

*E-mail: bul@niic.nsc.ru.

■ ACKNOWLEDGMENT

This work was partially supported by the French Embassy in Russia. We are grateful to Dr. V. S. Danilovich for the SEM measurements and Mr. A. V. Ischenko for the TEM measurements.

■ REFERENCES

(1) Endo, M.; Strano, M. S.; Ajayan, P. M. *Top. Appl. Phys.* **2008**, *111*, 13.
(2) Laurent, Ch.; Flahaut, E.; Peigney, A.; Rousset, A. *New J. Chem.* **1998**, *22*, 1229.
(3) Jong, W. J.; Lai, S. H.; Hong, K. H.; Lin, H. N.; Shih, H. C. *Diam. Relat. Mater.* **2002**, *11*, 1019.
(4) Rümmeli, M. H.; Schäffel, F.; Kramberger, C.; Gemming, T.; Bachmatiuk, A.; Kalenczuk, R. J.; Rellinghaus, B.; Büchner, B.; Pichler, T. *J. Am. Chem. Soc.* **2007**, *129*, 15772.
(5) Schäffel, F.; Rümmeli, M. H.; Kramberger, C.; Queitsch, U.; Mohn, E.; Kaltofen, R.; Pichler, T.; Büchner, B.; Rellinghaus, B.; Shultz, L. *Phys. Stat. Sol. (a)* **2008**, *205*, 1382.
(6) Danafar, F.; Fakhru'l-Razi, A.; Salleh, M. A. M.; Biak, D. R. A. *Chem. Eng. J.* **2009**, *155*, 37.
(7) Luo, G.; Li, Z.; Wei, F.; Xiang, F.; Deng, X.; Jin, Y. *Phys B: Condens. Matter.* **2002**, *323*, 314.
(8) Lee, C. J.; Park, J.; Yu, J. A. *Chem. Phys. Lett.* **2002**, *360*, 250.
(9) Wei, F.; Zhang, Q.; Qian, W.-Z.; Yu, H.; Wang, H.; Luo, G.-H.; Xu, G.-H.; Wang, D.-Z. *Powder Technol.* **2008**, *183*, 10.
(10) Koziol, K. K. K.; Ducati, C.; Windle, A. H. *Chem. Mater.* **2010**, *22*, 4904.
(11) Kumar, M.; Ando, Y. *J. Nanosci. Nanotechnol.* **2010**, *10*, 3739.
(12) Tessonier, J.-P.; Su, D. S. *ChemSusChem.* **2011**, *4*, 824.
(13) Ago, H.; Nakamura, K.; Uehara, N.; Tsuji, M. *J. Phys. Chem. B* **2004**, *108*, 18908.
(14) Magrez, A.; Seo, J. W.; Miko, C.; Hernádi, K.; Forró, L. *J. Phys. Chem. B* **2005**, *109*, 10087.
(15) Mionić, M.; Alexander, D. T. L.; Forró, L.; Magrez, A. *Phys. Stat. Sol. (b)* **2008**, *245*, 1915.
(16) Xu, Y.; Li, Z.; Dervishi, E.; Saini, V.; Cui, J.; Biris, A. R.; Lupu, D.; Biris, A. S. *J. Mater. Chem.* **2008**, *18*, 5738.
(17) Vander Wal, R. L.; Ticich, T. M.; Curis, V. E. *Carbon* **2001**, *39*, 2277.
(18) Hernadi, K.; Kónya, Z.; Siska, A.; Kiss, J.; Oszkó, A.; Nagy, J. B.; Kiricsi, I. *Mater. Chem. Phys.* **2003**, *77*, 536.
(19) Flahaut, E.; Peigney, A.; Bacsa, W. S.; Bacsa, R. R.; Laurent, Ch. *J. Mater. Chem.* **2004**, *14*, 646–653.
(20) Biris, A. R.; Lupu, D.; Dervishi, E.; Li, Z.; Xu, Y.; Trigwell, S.; Mişan, I.; Biris, A. S. *Phys. Lett. A* **2008**, *372*, 6416.
(21) Couteau, E.; Hernadi, K.; Seo, J. W.; Thiên-Nga, L.; Mikó, Cs.; Gaál, R.; Forró, L. *Chem. Phys. Lett.* **2003**, *378*, 9.
(22) Rümmeli, M. H.; Schäffel, F.; de los Arcos, T.; Haberer, D.; Bachmatiuk, A.; Kramberger, C.; Ayala, P.; Borowiak-Palen, E.; Adebimpe, D.; Gemming, T.; Leonhardt, A.; Rellinghaus, B.; Schultz, L.; Pichler, T.; Büchner, B. *Phys Stat Sol (b)* **2008**, *245*, 1939.
(23) Flahaut, E.; Peigney, A.; Laurent, Ch.; Rousset, A. *J. Mater. Chem.* **2000**, *10*, 249.
(24) Dupois, A.-C. *Progr. Mater. Sci.* **2005**, *50*, 929.
(25) Dervishi, E.; Li, Z.; Biris, A. R.; Lupu, D.; Trigwell, S.; Biris, A. S. *Chem. Mater.* **2007**, *19*, 179.
(26) Shlyakhova, E. V.; Yudanov, N. F.; Okotrub, A. V.; Shubin, Yu. V.; Yudanova, L. I.; Bulusheva, L. G. *Inorg. Mater.* **2008**, *44*, 213.
(27) Abdel-Kader, M. M.; El-Kabbany, F.; Taha, S.; Abosehly, M.; Tahoon, K. K.; El-Sharkawy, A. A. *J. Phys. Chem. Sol.* **1991**, *52*, 655.
(28) Gon, H. B. *J. Cryst. Growth.* **1990**, *102*, 501.
(29) Abbate, S.; Castiglione, F.; Lebon, F.; Longhi, G.; Longo, A.; Mele, A.; Panzeri, W.; Ruggirello, A.; Liveri, V. T. *J. Phys. Chem. B* **2009**, *113*, 3024.
(30) Torres, M. E.; Lopez, T.; Stockel, J.; Solans, X.; García-Vallés, M.; Rodrínguez-Castellón, E.; González-Silingo, C. *J. Solid State Chem.* **2002**, *163*, 491.
(31) Selvarajan, P.; Das, B. N.; Gon, H. B.; Rao, K. V. *J. Mater. Sci. Lett.* **1993**, *12*, 1210.
(32) Sahaya Shajan, X.; Mahadevan, C. *Cryst. Res. Technol.* **2005**, *40*, 598.
(33) Shlyakhova, E. V.; Yudanov, N. F.; Shubin, Yu.V.; Yudanova, L. I.; Bulusheva, L. G.; Okotrub, A. V. *Carbon* **2009**, *47*, 1701.
(34) Flahaut, E.; Bacsa, R.; Peigney, A.; Laurent, Ch. *Chem. Commun.* **2003**, 1442.
(35) Ravel, B.; Newville, M. *J. Synchrotron Radiat.* **2005**, *12*, 537.
(36) Newville, M. *J. Synchrotron Radiat.* **2001**, *8*, 322.
(37) Ambady, G. K. *Acta Crystallogr., Sect. B: Struct. Crystallogr. Cryst. Chem.* **1968**, *24*, 1548.
(38) Langell, M. A.; Anderson, M. D.; Carson, G. A.; Peng, L.; Smith, S. *Phys. Rev. B* **1999**, *59*, 4791.
(39) Dresselhaus, M. S.; Jorio., A.; Souza Filho, A. G.; Saito, R. *Philos. Trans. R. Soc. A* **2010**, *368*, 5355.
(40) Nii, H.; Sumiyama, Y.; Nakagawa, H.; Kunishige, A. *Appl. Phys. Express* **2008**, *1*, 064005.
(41) Meyer., J. C.; Paillet, M.; Michel, T.; Moréac, A.; Neumann, A.; Duesberg, G. S.; Roth, S.; Sauvajol, J.-L. *Phys. Rev. Lett.* **2005**, *95*, 217401.
(42) Gevko, P. N.; Okotrub, A. V.; Bulusheva, L. G.; Yushina, I. V.; Dettlaff-Weglikowska, U. *Phys. Solid State.* **2006**, *48*, 1007.
(43) Bulusheva, L. G.; Gevko, P. N.; Okotrub, A. V.; Lavskaya, Yu.V.; Yudanov, N. F.; Yudanova, L. I.; Abrosimov, O. G.; Pazhetnov, E. M.; Boronin, A. I.; Flahaut, E. *Chem. Mater.* **2006**, *18*, 4967.

(44) Zeng, F.; Zong, R. L.; Gu, Y. L.; Lv, F.; Pan, F.; Wang, F.; Yan, W. S.; He, B.; Xie, Y. N.; Liu, T. *Nucl. Instrum. Methods Phys. Res. B* **2007**, *260*, 547.
(45) Serov, T.; Nedoseykina, T.; Shvachko, T.; Kwak, C. *J. Power Sources* **2010**, *195*, 175.
(46) Puntes, V. F.; Krishnan, K. M.; Alivisatos, A. P. *Science* **2001**, *291*, 2115.
(47) de la Peña O'shea, V. A.; Ramírez de la Piscina, P.; Homs, N.; Aromí, G.; Fierro, J. L. G. *Chem. Mater.* **2009**, *21*, 5637.
(48) Sun, S.; Murray, C. B. *J. Appl. Phys.* **1999**, *85*, 4325.
(49) Kitakami, O.; Sato, H.; Shimada, Y.; Sato, F.; Tanaka, M. *Phys. Rev.B* **1997**, *56*, 13849.
(50) Hu, M.; Murakami, Y.; Ogura, M.; Maruyama, S.; Okubo, T. *J. Catal.* **2004**, *225*, 230.
(51) Kónya, Z.; Kiss, J.; Oszkó, A.; Siska, A.; Kiricsi, I. *Phys. Chem. Chem. Phys.* **2001**, *3*, 155.
(52) Narkiewicz, U.; Podsiadły, M.; Jędrzejewski, R; Pełech, I. *Appl. Catal., A* **2010**, *384*, 27.